Climate Dynamics (2026) 64:426
https://doi.org/10.1007/s00382-026-08378-8

ORIGINAL ARTICLE

Application of the unified extreme value theory to global extreme precipitation anomaly events

Yuting Xin[1] · Jianping Li[1,2] · Wei Ban[1]

Received: 5 June 2026 / Accepted: 31 August 2026

Abstract
Historical changes in extreme precipitation and their return-period characteristics have been widely investigated. Most previous analyses have focused on extreme precipitation indices or extreme-value series. However, for global annual precipitation anomalies, the long-term evolution of wet and dry anomalies remains insufficiently characterized within a unified statistical framework. Based on global land annual total precipitation data for 1891–2020, this study applies the Unified Extreme Value Theory (UEVT) to systematically examine changes in the return levels, occurrence counts, and spatial patterns of extreme wet and dry precipitation anomaly events. The results show that both 10-year and 50-year events exhibit a consistent 'wet-gets-wetter and dry-gets-drier' tendency over the past 130 years. The return level of 10-year extreme wet anomalies increases from 17.4 mm to 40.8 mm, and events with the same return period occur more frequently in recent decades. Spatially, the strengthening of 10-year extreme wet anomalies is more widespread, with nearly 70% of global land showing an increase, whereas extreme dry anomalies intensify over about 57.2% of the land area. The 50-year events generally retain this wet-dry contrast, although their spatial extent is slightly smaller and their local changes are stronger. Regional analyses indicate that wet anomalies strengthen more markedly in mid- to high-latitudes and monsoon-affected regions, whereas dry anomalies intensify more prominently in arid and semi-arid regions. By using a unified probabilistic framework, this study reveals the co-evolution of global extreme precipitation anomalies in terms of intensity, occurrence frequency, and spatial structure.

Keywords Return period · Return level · Unified extreme value theory · Extreme precipitation anomalies

1 Introduction

The global hydrological cycle is highly sensitive to climate changes, and variations in precipitation anomalies are among its most direct and complex manifestations. Previous studies have shown that increases in atmospheric moisture content and evaporative demand under warming jointly contribute to intensified heavy precipitation, rising drought risk, and amplified wet-dry fluctuations (Held and Soden 2006; Trenberth 2011; O'Gorman 2015; Gebrechorkos et al. 2025). In addition, precipitation variability has increased significantly over most global land areas during the past century, suggesting an expansion of precipitation anomalies toward both wet and dry extremes (Zhang et al. 2024a, b). Extreme wet and dry precipitation anomalies are closely linked to floods, droughts, and water-resource security, and they also affect ecosystem stability and socioeconomic activities through changes in soil moisture, runoff generation, and land–atmosphere water exchange (IPCC 2021; Trenberth and Asrar 2014; Huang et al. 2017; Xie et al. 2020). Phenomena such as concurrent droughts and floods and abrupt drought-flood transitions indicate that wet and dry precipitation anomalies may occur successively or alternately within a short period, leading to compound risks that often exceed those associated with individual wet or dry anomaly events (Wu et al. 2006a, 2006b; Tan et al. 2023; Su et al. 2024; He et al.

✉ Jianping Li
ljp@ouc.edu.cn

1 Frontiers Science Center for Deep Ocean Multi-Spheres and Earth System (DOMES)/Key Laboratory of Physical Oceanography/Academy of Future Ocean/College of Oceanic and Atmospheric Sciences/Center for Ocean Carbon Neutrality, Ocean University of China, Qingdao 266100, China

2 Laboratory for Ocean Dynamics and Climate, Qingdao Marine Science and Technology Center, Qingdao 266237, China

2025). Therefore, identifying the long-term and global-scale changes in these two types of anomaly events, as well as their differences, is essential for understanding how hydrological anomalies translate into climate-related risks.

Previous studies have examined historical changes in precipitation anomalies and related extreme events across global, regional, and multiple temporal scales. Observational analyses indicate that long-term precipitation changes do not simply reflect a globally uniform intensification, but instead exhibit pronounced spatial heterogeneity. Heavy precipitation events have continued to intensify in many regions, while precipitation deficits and drought anomalies have also increased in a number of areas, indicating that changes in the hydrological cycle are expressed on both the wet and dry sides of precipitation anomalies, with marked regional differences (Donat et al. 2016; Sun et al. 2021; Chen et al. 2025; Yate and Ren 2025), This regional disparity is also consistent with the understanding that extreme precipitation events are jointly modulated by moisture transport, vertical motion, air-sea interactions, and synoptic-scale circulation processes(Sun et al., 2023; Zhao et al. 2024; Li et al. 2026). Methodologically, existing studies have mainly relied on two types of approaches. One group uses extreme precipitation indices or drought indices to describe and detect trends in heavy precipitation, consecutive dry days, and precipitation deficits (Alexander et al. 2006; Donat et al. 2013; Dunn et al. 2024; Vicente-Serrano et al. 2010). The other group applies conventional extreme value theory to fit probability distributions to extreme-value series and thereby estimate changes in return periods and return levels (Katz et al. 2002; Kharin and Zwiers 2005; Westra et al. 2013; Gründemann et al. 2023; Jorgensen and Nielsen-Gammon 2024; Wehner et al. 2024; Li et al. 2025). These studies have laid an important foundation for understanding the historical evolution of precipitation anomalies and related extremes, and have established the general understanding that heavy precipitation is intensifying, drought risk is increasing, and regional differences are substantial.

Although precipitation anomalies and related extreme events have been characterized from different perspectives, existing analyses commonly examine wet and dry anomalies separately using different statistical objects. For wet anomalies, studies usually focus on heavy precipitation events themselves, or use metrics such as occurrence frequency, record-breaking rates, and return levels of rare rainfall events to describe their changes (Benestad et al. 2024; Devò et al. 2025). In contrast, dry anomalies are more often characterized using drought severity, drought recovery probability, and compound drought-heat events to represent precipitation deficits and their persistent impacts (Zhang et al. 2024a, b; Fan et al. 2024; Chen et al. 2025; Zhuang et al. 2024). As a result, although changes in wet and dry anomalies have been investigated separately, their return periods, intensities, and long-term evolution are difficult to compare directly because the two types of anomalies are usually defined using different indicators and statistical objects. For annual precipitation anomalies, however, wet and dry events both arise from deviations of annual total precipitation from the climatological mean. This provides a basis for characterizing the two types of events within a unified probabilistic framework.

To address this gap, this study starts from annual total precipitation anomalies and applies the unified extreme value theory to quantify the return periods and return levels of extreme wet and dry precipitation anomaly events within a common probabilistic framework. We focus on three questions: how return levels change for events with different return periods; whether events with the same return period have become more frequent; and how these changes differ spatially across global land areas and the Intergovernmental Panel on Climate Change Sixth Assessment Report (IPCC AR6) reference regions. Through this analysis, we aim to reveal the co-evolution of extreme wet and dry precipitation anomalies and to provide a unified statistical perspective for understanding long-term changes in global extreme precipitation anomalies.

2 Data and methods

2.1 Datasets

This study uses the GPCC Full Data Monthly Product Version 2022, provided by the Global Precipitation Climatology Centre (GPCC) of the German Weather Service (DWD). The dataset has a spatial resolution of 2.5° × 2.5°, a monthly temporal resolution, and covers the period 1891–2020. It is constructed from rain-gauge observations and has been widely used in studies of global and regional precipitation variability (Becker et al. 2013; Schneider et al. 2022). Monthly precipitation was first summed from January to December to obtain annual total precipitation. Annual precipitation anomalies were then calculated as

$$P'_y = P_y - \overline{P}_{1891-1940} \quad (1)$$

where P'_y is the annual precipitation anomaly in year y, P_y is the annual total precipitation in that year (or the area-averaged annual precipitation within an IPCC AR6 region for the regional analysis), and $\overline{P}_{1891-1940}$ is the mean annual precipitation during 1891–1940. Following the general practice adopted in the IPCC AR6 of using an early period of approximately 50 years as the reference baseline, the first 50 years of the GPCC record (1891–1940) were selected as the fixed early-climate reference period for constructing the annual precipitation anomaly series throughout the study period. Using a 50-year mean reduces the influence of interannual and decadal climate variability and provides a relatively stable historical reference. Because the method relies on the temporal variability of precipitation anomalies, several grid points with insufficient variability or evident abnormal values were screened before the analysis. In the early part of the record, some grid points show nearly constant precipitation for consecutive years, particularly in high-latitude regions, leading to extremely small variance; in addition, a few grid points contain anomalously large values in individual years. To improve the robustness of the results while maintaining a consistent sample length, a standard-deviation screening was applied to the first 20 years of annual total precipitation at each grid point. Let the annual precipitation series during the first 20 years be

$$P_1, P_2, \dots, P_{20}$$

and its standard deviation be defined as

$$\sigma = \sqrt{\frac{1}{20}\sum_{i=1}^{20}\left(P_i - \overline{P}\right)^2}, \overline{P} = \frac{1}{20}\sum_{i=1}^{20} P_i \tag{2}$$

where $\overline{P}$ is the mean annual precipitation during the first 20 years. When $\sigma < 2mm$, the grid point is regarded as invalid and is set to missing in the subsequent analysis. To assess the sensitivity of the results to the selected threshold, the grid-based return-level analysis was additionally repeated using standard-deviation thresholds of 1 and 3 mm, while all other calculation settings were kept unchanged. This screening was designed to identify and exclude abnormal grid points where precipitation anomalies remained nearly unchanged during the first 20 years and thus lacked meaningful interannual variability, thereby reducing the influence of unreliable precipitation records on the subsequent analysis of extreme-value distributions and the estimation of return levels and return periods.

To assess the consistency of the main conclusions across datasets, the CRU TS v4.05 monthly precipitation dataset (Harris et al. 2020) was additionally analyzed. This station-based gridded land precipitation dataset has a spatial resolution of 0.5° × 0.5° and covers the period 1901–2020. The same annual aggregation, anomaly calculation, and extreme value analysis were applied to CRU, with its first 50 years (1901–1950) used as the reference period. CRU was used as an independent cross-dataset consistency assessment, whereas GPCC remained the primary dataset because of its longer temporal coverage.

2.2 Unified extreme value theory

Annual precipitation anomalies are calculated relative to the 1891–1940 mean, as described in Sect. 2.1, and are used as the input series for the analysis. The Unified Extreme Value Theory (UEVT) developed by Ban and Li (2026) is then applied to characterize the occurrence probability, return period, and intensity of extreme wet and dry precipitation anomaly events within a common statistical framework. Positive anomalies denote wet events, whereas negative anomalies denote dry events; the two types of events therefore correspond to positive and negative departures of annual total precipitation from the climatological mean, respectively.

The return period T is defined as the average time interval required for an event to recur. If a given type of event occurs m times in a time series of length N, its occurrence frequency can be written as

$$f = \frac{m}{N} \tag{3}$$

and the corresponding return period is defined as the inverse of the frequency:

$$T = \frac{1}{f} = \frac{N}{m} \tag{4}$$

The return level denotes the event intensity associated with a given return period, that is, the corresponding quantile. An event with a return period of T is referred to as a T-year event. Following these definitions, an independent and identically distributed annual precipitation anomaly series can be expressed as

$$X = \{x_1, x_2, \dots, x_n\}$$

According to the sign of the anomaly, the series is divided into positive anomalies (wet events) and negative anomalies (dry events), representing anomalous high andlow annual precipitation, respectively. The occurrence probabilities of wet and dry events are then defined as

$$P(X \le x) = F(x), x \le 0 \tag{5a}$$

$$P(X \ge x) = 1 - F(x), x > 0 \tag{5b}$$

where $F(x)$ is the cumulative distribution function of the annual precipitation anomaly series X. Its empirical form is

$$F(x) = \sum_{x_i \le x} p_i \tag{6}$$

Accordingly, the return periods of wet and dry precipitation anomaly events can be written in an unified form as

$$RP(x) = \begin{cases} \dfrac{1}{P(X \geq x)}, & x > 0 \\ \dfrac{1}{P(X \leq x)}, & x \leq 0 \end{cases} \tag{7}$$

where $RP(x)$ is the return period of the event and x is the corresponding return level. This formulation establishes the relationship between return period and return level for extreme wet and dry precipitation anomaly events within a unified statistical framework.

To investigate the temporal evolution of extreme precipitation anomaly events, a 50-year moving-window approach is applied to the annual precipitation anomaly series. Let L_w denotes the moving-window length and T represents the return period. The empirical estimation requires $L_w \geq T$. Because both 10-year and 50-year events are examined, $L_w = 50$ years was selected as the minimum window length that satisfies this requirement while retaining relatively high temporal resolution. Tests with longer windows yielded smoother estimates and minor numerical differences but did not alter the main conclusions. Within each moving window, the return period–return level relationship is estimated separately for wet and dry events. The return level associated with a given return period T is defined as the critical intensity in that window, namely the intensity of a T-year extreme wet or dry precipitation anomaly event. If the return level corresponding to T in the k-th moving window is denoted as $x_k(T)$, then the sequence $x_k(T)$, obtained as the window advances year by year, represents the time-varying critical intensity for a fixed return period and is used to characterize the long-term intensity evolution of extreme wet and dry precipitation anomaly events. In addition, the critical intensity during the reference period is used as a fixed threshold, and the number of events exceeding this threshold in each moving window is counted to assess changes in the occurrence frequency of events with the same return period.

2.3 Regional division

To examine regional differences in extreme precipitation anomaly events under different climatic backgrounds, the IPCC AR6 reference regions are used as the regional framework (Iturbide et al. 2020). The abbreviations, names, and attributes of these regions are listed in Supplementary Table 1.

3 Temporal evolution of 10-year and 50-year extreme precipitation anomaly events

The temporal evolution of return levels indicates that both 10-year and 50-year extreme precipitation anomaly events exhibit concurrent intensification of wet anomalies and dry anomalies (Fig. 1a, c). For the 10-year event, the return level of extreme wet precipitation anomalies increases from about 17.4 mm in the early period to 40.8 mm in recent decades,

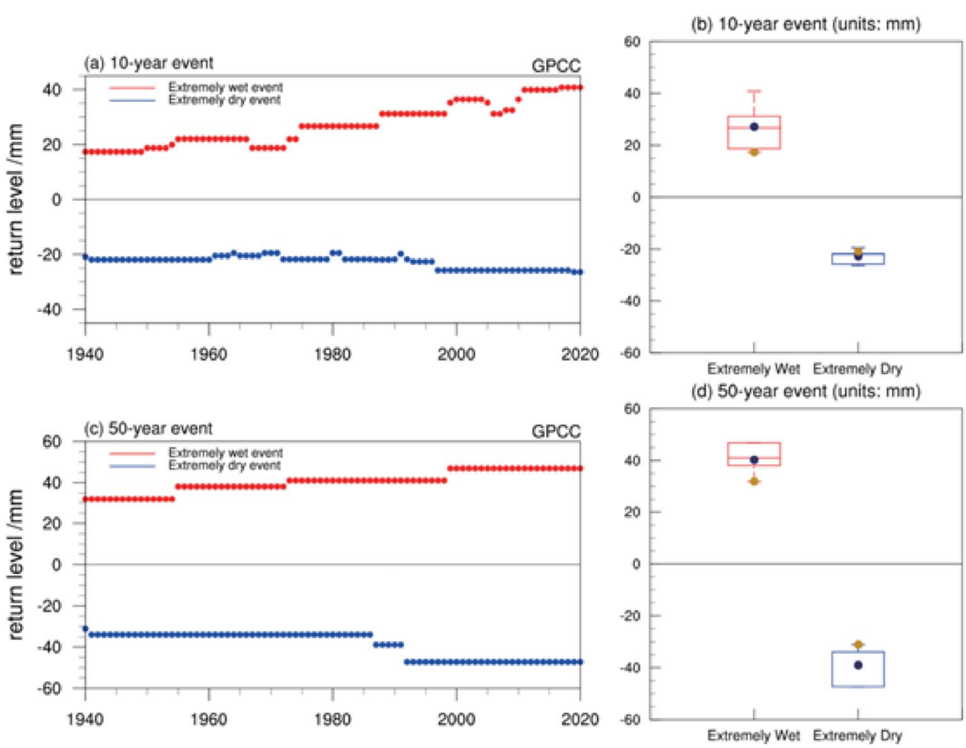

Fig. 1 Temporal evolution and statistical characteristics of return levels for extreme precipitation anomaly events derived from the globally averaged annual total precipitation anomaly series over land based on the GPCC dataset (1891–2020). **a** Time series of return levels for extremely wet (red) and extremely dry (blue) precipitation anomaly events with a 10-year return period. Return levels are estimated using a 50-year moving window, and the x-axis denotes the ending year of each window. **b** Box plots of return levels from the 81 moving windows shown in **a**. The boxes and whiskers represent the minimum, 25th percentile, median, 75th percentile and maximum values. Yellow dots indicate the baseline return levels for the reference period (1891–1940), whereas blue dots denote the mean critical intensities across all moving windows. **c** Same as **a**, but for the 50-year return period. **d** Same as **b**, but for the 50-year return period

corresponding to an increase of approximately 134.5%. The trend is statistically significant, indicating a sustained increase in the positive anomaly magnitude associated with the same return period. In contrast, the 10-year extreme dry anomaly decreases from about −20.9 to −26.4 mm, representing a reduction of approximately 26.3%. This change is relatively gradual and does not reach statistical significance, suggesting that the dry-side signal is weaker and less stable than the wet-side signal at the global land mean scale.

For the 50-year event, the return level of extreme wet anomalies increases from about 31.9 to 46.9 mm, with an overall increase of approximately 47.0%. The stepwise upward evolution of the moving-window estimates suggests a persistent intensification of rare wet anomalies under different background climate states. The return level of extreme dry anomalies decreases from about −31.1 to −47.3 mm, corresponding to a reduction of approximately 52.1%. Notably, the dry return level shows a marked downward shift when the ending year of the moving window approaches the 1990s, after which it remains at a relatively low level.

The box plots further illustrate the distribution of return levels across different moving windows (Fig. 1b, d). The boxes and whiskers represent the distribution of return levels for a fixed return period across all windows, while the yellow and blue dots denote the baseline return level and the mean critical intensity, respectively. For the 10-year event, the baseline return level of extreme wet anomalies is about 17.4 mm, whereas the mean critical intensity is about 27.1 mm, representing an increase of approximately 55.7% relative to the reference period. For extreme dry anomalies, the baseline return level changes from −20.9 mm to a mean critical intensity of about −22.8 mm, corresponding to a change of approximately 9.1%.

For the 50-year event, the baseline return level of extreme wet anomalies is about 31.9 mm, and the mean critical intensity is about 40.2 mm, corresponding to an increase of approximately 26.0%. For extreme dry anomalies, the baseline return level changes from −31.1 to about −39.0 mm, with a relative change of approximately 25.4%. Overall, the wet anomalies show a wider box-plot range and a larger mean increase under the 10-year return period, whereas the intensification of dry anomalies is more pronounced under the 50-year return period. These results indicate an asymmetric response of wet and dry anomalies across different return periods.

A comparison between the 10-year and 50-year events shows that extreme wet and dry anomalies in the global annual precipitation anomaly series do not evolve symmetrically. The wet side exhibits a clearer and more robust long-term increase under the 10-year return period, whereas the dry-side intensification is more evident for the 50-year event. This asymmetry indicates that the long-term changes in extreme precipitation anomalies involve not only a simultaneous expansion toward both tails of the distribution, but also differences in magnitude, trend stability and dispersion between wet and dry anomalies. The intensification of wet anomalies is consistent with the thermodynamic effect of increased atmospheric moisture under warming, while the strengthening of dry anomalies may be linked to changes in large-scale moisture balance and an amplification of hydroclimatic variability (Held and Soden 2006; Tan et al. 2023; Gebrechorkos et al. 2025). Taken together, these results suggest a two-sided expansion of global precipitation anomalies over the past century, with wet anomalies becoming wetter and dry anomalies becoming drier, rather than a change confined to only one tail of the distribution.

The changes in return levels described above characterize the long-term evolution of event intensity under fixed return periods. From a climate-risk perspective, however, it is equally important to determine whether events that were defined as multi-year events in the reference climate have become more frequent under later climate conditions. We therefore use the return levels for the reference period as fixed thresholds and count the number of exceedances within each 50-year moving window, thereby evaluating the temporal evolution of event occurrence under the same return-period definition.

The results show an overall increase in the number of occurrences of reference-period multi-year extreme precipitation anomaly events in later 50-year windows (Fig. 2). For the 10-year event (Fig. 2a), extreme wet anomalies occur about five times in the early window (1891–1940), but increase to about 14 occurrences in the recent window (1971–2020). Over the same period, the number of extreme dry anomalies increases from about five to about nine. Thus, within a fixed 50-year window, both 10-year wet and dry anomaly events defined by the reference climate have become more common. The increase is larger for wet anomalies, while the rise in dry anomalies is mainly concentrated in the later windows.

A similar pattern is found for the 50-year event (Fig. 2b). Extreme wet anomalies increase from about one occurrence in the early window (1891–1940) to about eight occurrences in the recent window (1971–2020), whereas extreme dry anomalies increase from about one to about four occurrences. This indicates that events that were relatively rare in the reference period have occurred more frequently under later climate conditions, implying a shortening of their effective recurrence intervals. As for the 10-year event, the increase is more pronounced for wet anomalies, although dry anomalies also show a clear increase in the later period.

Overall, the number of occurrences of extreme precipitation anomaly events increases within fixed 50-year

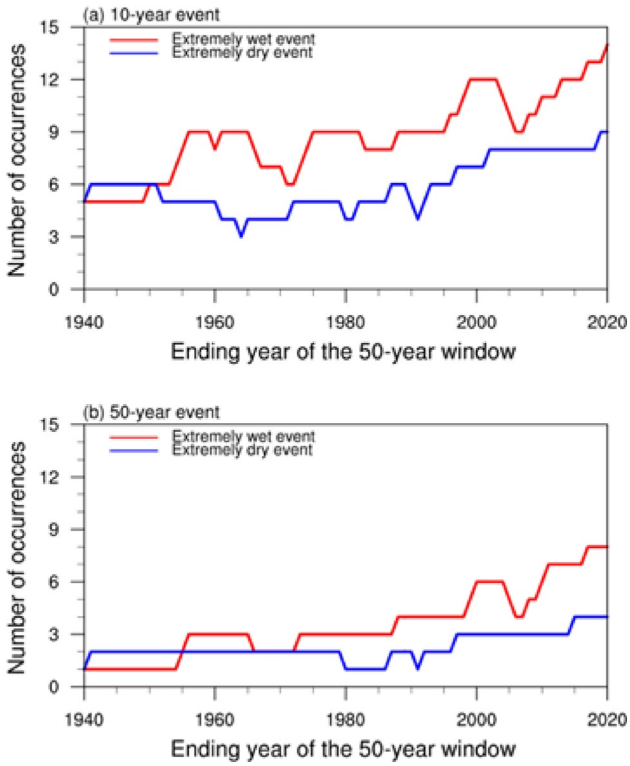

Fig. 2 Temporal evolution of the number of occurrences of extreme precipitation anomaly events derived from the globally averaged annual precipitation anomaly series over land based on the GPCC dataset (1891–2020). **a** Number of occurrences of extremely wet (red) and extremely dry (blue) precipitation anomaly events with a 10-year return period within each 50-year moving window. The period 1891–1940 is used as the reference, and the x-axis denotes the ending year of each moving window. **b** Same as **a**, but for the 50-year return period

windows for both return periods, with a stronger increase for wet anomalies than for dry anomalies. Together with the increase in return levels, these results indicate that changes in global land-mean extreme precipitation anomalies are expressed not only as stronger events under fixed return periods, but also as more frequent occurrences of reference-period multi-year events. This points to an increase in extreme hydroclimatic risk along both the intensity and occurrence dimensions.

4 Spatial patterns of changes in return levels of extreme precipitation anomaly events

Figure 3 shows a consistent statistical relationship between the intensity of extreme annual precipitation anomaly events and the local climatological mean annual precipitation during the reference period. Grid points with larger mean annual precipitation generally exhibit larger positive anomalies for extreme wet events and larger absolute negative anomalies for extreme dry events. The absolute regression slopes are larger for 50-year events than for 10-year events, indicating that rarer events are more sensitive to the background precipitation climatology. However, the substantial scatter also suggests that the mean precipitation climatology explains only part of the spatial variability in extreme anomaly intensity.

The spatial distribution of changes in 10-year return levels during 1971–2020 relative to 1891–1940 shows widespread strengthening of extremely wet precipitation anomalies over global land (Fig. 4). Increases are concentrated mainly in the Northern Hemisphere mid- to high-latitudes, including northern and eastern Europe, western Siberia, eastern North America, and East Asia, where local values exceed 100–150 mm. Pronounced increases also occur in Southeast Asia, southeastern South America, and northern Australia, whereas decreases are more scattered across parts of the low latitudes and subtropics. Consistently, the zonal mean shows a continuous positive signal over the Northern Hemisphere mid- to high-latitudes, while the Southern Hemisphere signal is concentrated mainly between 10° and 40°S (Fig. 4b). Overall, wet-event return levels increase across approximately 69.3% of the effective global land area and decrease across 30.7% (Fig. 4a).

The changes in 10-year extremely dry precipitation anomalies exhibit greater regional heterogeneity (Fig. 4d). Because dry-event return levels are negative, a further decrease represents an intensification of dry anomalies, whereas a positive change represents a weakening. Intensification occurs mainly in central and southern Africa, South and Southeast Asia, Indonesia and adjacent Maritime Continent regions, parts of South America, and localized areas of Australia, with local change magnitudes exceeding 200 mm. The zonal mean indicates that these changes are concentrated in the low latitudes and parts of the Southern Hemisphere, while dry anomalies generally change only weakly or become weaker over the Northern Hemisphere mid- to high latitudes. Decreased dry-event return levels cover 57.2% of global land, indicating an overall intensification of dry anomalies, although with less spatial extent and continuity than the strengthening of wet anomalies (Fig. 4c).

The wet and dry patterns exhibit both regional correspondence and asymmetry. Southeast Asia, parts of Australia, and central-to-southern Africa show simultaneous strengthening of wet and dry anomalies, indicating an expansion of both tails of the annual precipitation anomaly distribution. By contrast, eastern North America and the region extending from northern Europe to western Siberia exhibit stronger wet anomalies but weaker dry anomalies, suggesting a shift toward the wet side of the distribution.

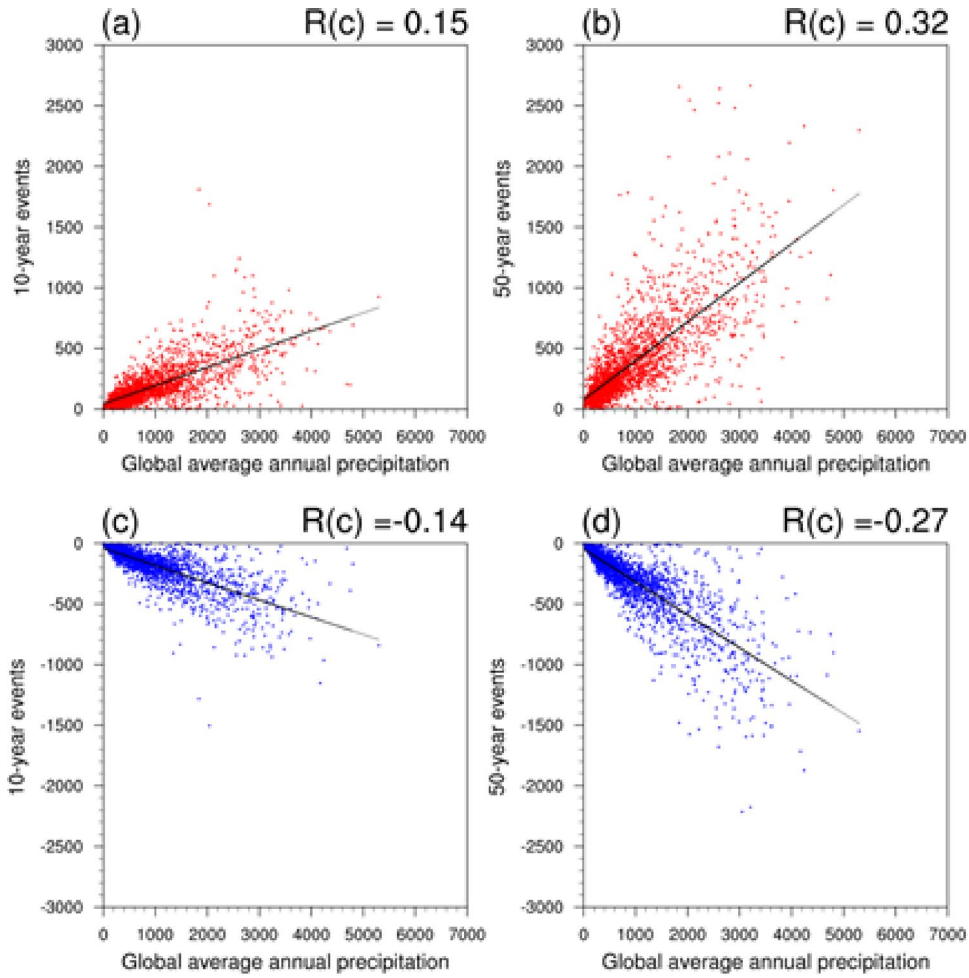

Fig. 3 Relationship between the intensity of extreme annual precipitation anomaly events and the climatological mean annual precipitation at each land grid point during the reference period (1891–1940) based on the GPCC dataset. **a** Extremely wet precipitation anomaly events with a 10-year return period: the x-axis represents the mean annual precipitation at each grid point, while the y-axis represents the return-level anomaly of extremely wet events (mm). **c** Same as **a**, but for extremely dry precipitation anomaly events. The solid black line denotes the univariate linear regression fit, and R(c) is the regression slope. **b** Same as **a**, but for the 50-year return period. **d** Same as **c**, but for the 50-year return period

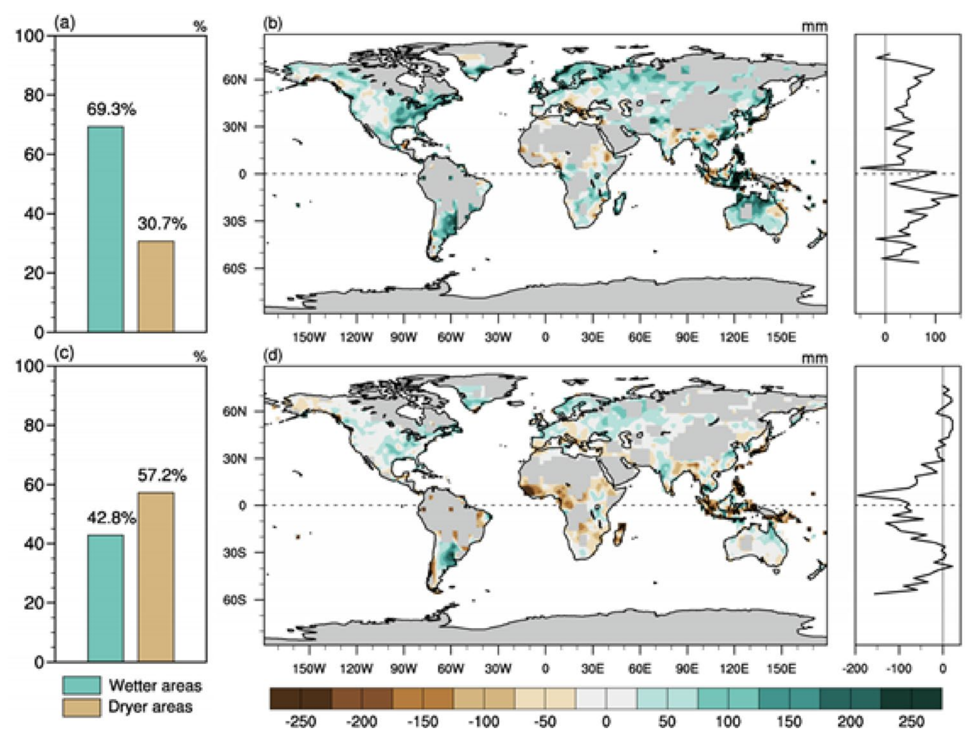

Fig. 4 Characteristics of changes in the 10-year return levels of extreme annual precipitation anomalies over global land during the recent 50-year period (1971–2020) relative to the reference period (1891–1940). **a** Fraction of global land area with increasing (green) and decreasing (tan) return levels for extremely wet precipitation anomaly events. **b** Spatial distribution of return-level changes (mm) for extremely wet events; the curve on the right indicates the corresponding zonal mean. **c** Same as **a**, but for extremely dry precipitation anomaly events. **d** Same as **b**, but for extremely dry events

The spatial pattern of 50-year events is broadly consistent with that of 10-year events, but the affected areas are slightly smaller (Fig. 5). Increased wet-event return levels cover 63.2% of the effective global land area, compared with 69.3% for 10-year events, and remain pronounced in Southeast Asia, East Asia, Australia, and parts of the Northern Hemisphere mid- to high latitudes (Fig. 5a, b). Decreased dry-event return levels account for 53.7% of global land, compared with 57.2% for 10-year events, and are concentrated mainly in Southeast Asia, low- to mid-latitude Africa, and other tropical and subtropical land regions (Fig. 5c, d). In contrast, changes in the Northern Hemisphere mid- to high latitudes are generally weaker or indicate a weakening of dry anomalies.

Overall, both return periods show strengthened wet anomalies and intensified dry anomalies over most global land areas, but their spatial characteristics differ. The 10-year events exhibit broader and more spatially continuous changes, whereas the 50-year events affect smaller areas but show stronger local changes. This contrast indicates that the spatial evolution of extreme precipitation anomalies depends on both spatial coverage and return-period-related differences in local magnitude.

To further assess the stability of the spatial results, we repeated the analysis using standard-deviation thresholds of 1, 2, and 3 mm. The estimated land-area proportions varied only slightly, with a maximum difference of 1.6 percentage points among the three thresholds, while the overall wet and dry patterns for both return periods remained consistent. This indicates that the main conclusions are not sensitive to reasonable variations in the screening threshold (Supplementary Table S2).

5 Regional characteristics of extreme precipitation anomaly events across IPCC AR6 reference regions

The time series and trend slopes for the IPCC AR6 reference regions further reveal substantial regional differences in extreme wet and dry precipitation anomaly events (Figs. 6 and 7). Overall, return levels of wet anomalies show increasing trends in most regions. For the 10-year events, more than two-thirds of the IPCC land regions exhibit positive trends, with relatively pronounced increases in NEU, EEU, WSB, RFE, EAS, SEA and NAU; some of these trends are statistically significant at the 0.05 level. This indicates that multi-year extreme wet anomalies have intensified in several mid- to high-latitude regions and in regions influenced by monsoonal precipitation. By contrast, changes in dry anomalies are more spatially heterogeneous. For the 10-year events, enhanced dry anomalies occur mainly in SCA, NWS, SAM, WAF, SEA and SAU, whereas WNA, ENA, NEU, WCE, ESB and NZ show weakened dry anomalies or relatively weak changes.

Clear differences are also found between return periods. Compared with the 10-year events, the 50-year events show a more spatially uneven response, with stronger local changes in some regions and, in some cases, changes in the opposite direction to those of the 10-year events. This

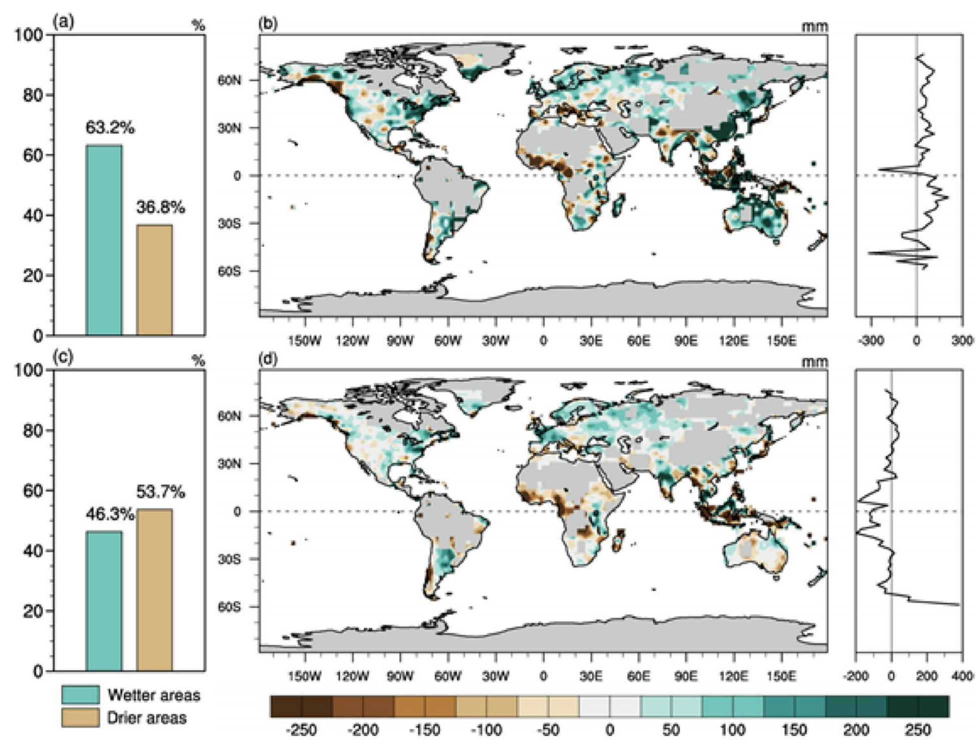

Fig. 5 Same as Fig. 4, but for 50-year events

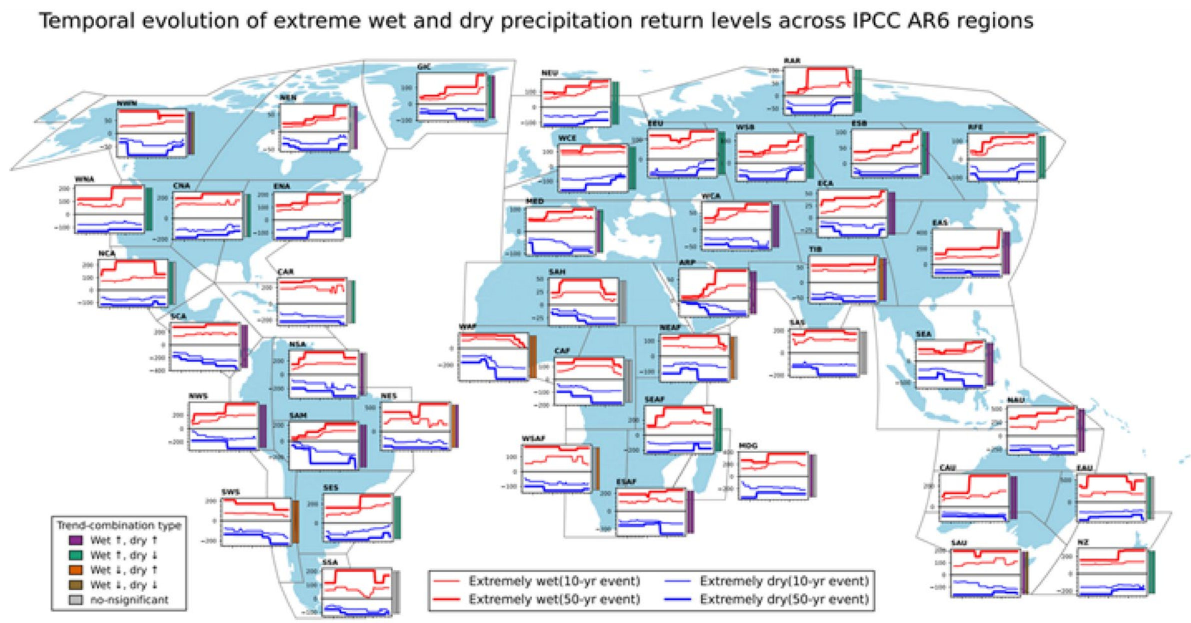

Fig. 6 Temporal evolution of return levels of extreme wet and dry precipitation anomalies across the IPCC AR6 reference region, calculated separately from the area-weighted annual precipitation anomaly series of each region during 1891–2020 (units: mm). Red and blue curves represent extremely wet and extremely dry precipitation anomaly events, respectively. Thin solid lines denote 10-year return-period events, while thick solid lines denote 50-year return-period events. Return levels are calculated using a 50-year moving window, and the x-axis indicates the ending year of each window. The two vertical color bars to the right of each inset indicate the trend-combination types for the 10-year and 50-year events, respectively, with colors defined in the legend and Tables 1 and 2

suggests that extreme precipitation anomalies of different intensity levels do not respond uniformly to changes in the climatic background. The trend-combination classification further shows that NWS, SAM, ESAF, EAS, SEA, NAU and CAU are typical regions where both wet and dry anomalies intensify, indicating a widening of both the positive and negative tails of annual precipitation anomalies. In contrast, WNA, ENA, NEU, WCE, ESB, RFE and NZ are characterized by enhanced wet anomalies but weakened dry anomalies, suggesting a shift of the anomaly distribution toward the wet side. The complete regional classifications are given in Tables 1 and 2. Overall, the classifications based on the number of IPCC AR6 regions are consistent with the grid-cell area statistics shown in Figs. 4 and 5: both indicate that wet-anomaly intensification is more widespread, whereas dry-anomaly intensification is more regionally selective. These results suggest that the spatial changes identified in this study are robust across different statistical scales, with regional extreme precipitation anomalies characterized by both widespread wet-anomaly intensification and more selective dry-anomaly intensification Tables 3 and 4.

Tables 3 and 4 further quantify the overall deviations of extreme wet and dry annual precipitation anomaly events from the reference period across the IPCC AR6 reference regions, in terms of baseline return levels, mean critical intensities and relative changes. In most regions, the mean critical intensity of wet anomalies is higher than the baseline return level, indicating relatively widespread regional consistency in wet-anomaly intensification. Typical regions that pass the trend test, such as NEU, EEU, WSB, RFE and EAS, show not only significant upward trends but also large positive relative changes, further confirming the persistent intensification of extreme wet anomalies in these regions. In contrast, although dry anomalies shift toward more negative mean critical intensities in several regions, their magnitudes and statistical significance are more spatially heterogeneous, indicating that dry-anomaly intensification is not spatially uniform. Compared with the 10-year events, the 50 year events show stronger local changes in some regions but fewer regions with significant trends, suggesting that higher-return-period events are more regionally dependent and exhibit more complex spatial responses. Taken together, the regional time series, trend tests and tabulated quantitative results show that long-term changes in extreme precipitation anomalies at the regional scale are characterized by widespread wet-anomaly intensification and selective dry-anomaly intensification in specific regions.

To assess the sensitivity of these results to dataset choice, the analysis was repeated using CRU TS v4.05 (Supplementary Figs. S1–S4). Because GPCC and CRU have different starting years and first 50-year reference periods, the comparison focuses on long-term tendencies and regional patterns rather than exact numerical agreement. Both datasets show significant increases in the 10-year and 50-year return

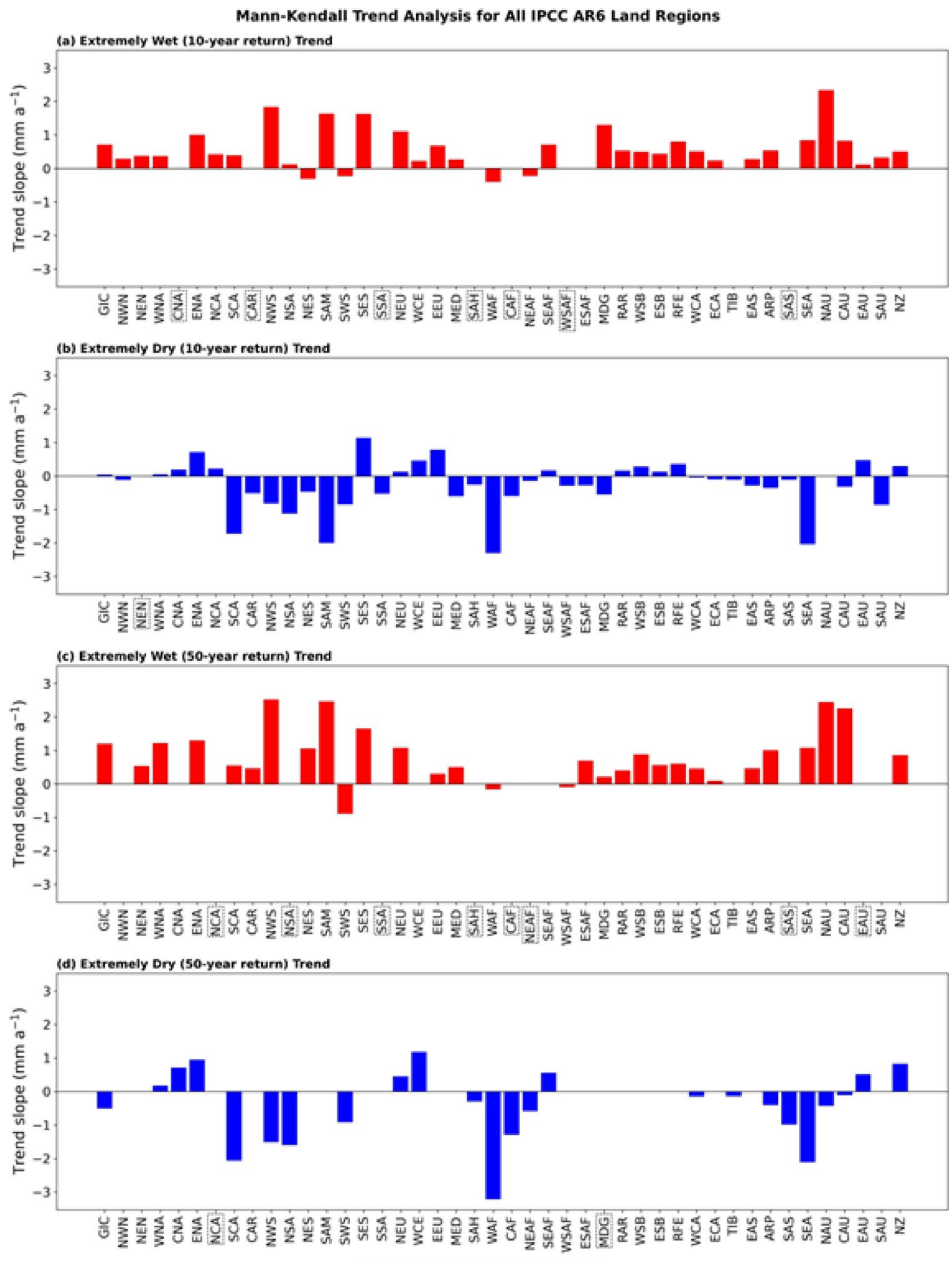

Fig. 7 Trends in return levels of extreme precipitation anomalies for 10-year and 50-year events across IPCC AR6 reference regions. **a** Extremely wet precipitation anomaly events (red bars) for the 10-year return period. Bar height denotes Sen's slope (mm a^{-1}), while the statistical significance of the trend is assessed using the Mann–Kendall test. Regions enclosed by dashed boxes along the horizontal axis indicate non-significant trends ($p \geq 0.05$), whereas regions without dashed boxes indicate statistically significant trends ($p<0.05$). **b** Same as **a**, but for extremely dry precipitation anomaly events (blue bars). **c** Same as **a**, but for the 50-year return period. **d** Same as **b**, but for the 50 year return period

levels and occurrence frequencies of extreme wet anomalies. For dry anomalies, the 10-year changes are weak and statistically insignificant, whereas the 50-year results show stronger return-level magnitudes in recent windows relative to the reference period, accompanied by a modest increase in occurrence frequency. At the regional scale, GPCC and CRU yield the same wet–dry trend-combination classification in 56.8% and 63.6% of the IPCC AR6 land regions for the 10-year and 50-year events, respectively, with 72.7% agreeing for at least one return period. Overall, the comparison supports the stability of the wet-side intensification and provides qualitatively consistent evidence for changes in rarer dry anomalies.

6 Conclusions and outlook

This study characterizes the long-term changes in extreme wet and dry precipitation anomaly events within a unified statistical framework, thereby avoiding the limited comparability that arises when the two types of events are described using different indices or statistical objects. The results show that, over the past century, global extreme

Table 1 Trend-combination types of 10-year extreme wet and dry precipitation anomaly events across the IPCC AR6 reference regions, based on the trend test results shown in Fig. 7

Trend-combination type	Regions	Number	Fraction of 44 regions
Both wet and dry anomalies intensify	NWN, SCA, NWS, NSA, SAM, MED, ESAF, MDG, WCA, ECA, EAS, ARP, SEA, NAU, CAU, SAU	16	36.4%
Wet anomalies intensify, dry anomalies weaken	GIC, WNA, ENA, NCA, SES, NEU, WCE, EEU, SEAF, RAR, WSB, ESB, RFE, EAU, NZ	15	34.1%
Wet anomalies weaken, dry anomalies intensify	NES, SWS, WAF, NEAF, TIB	5	11.4%
Both wet and dry anomalies weaken	None	0	0
At least one side is not significant	NEN, CNA, CAR, SSA, SAH, CAF, WSAF, SAS	8	18.2%

The full names and attributes corresponding to the IPCC AR6 regional abbreviations are provided in Table S1 of the Supplementary Material

Table 2 Same as Tab. 1, but for a 50 year event

Trend-combination type	Regions	Number	Fraction of 44 regions
Both wet and dry anomalies intensify	GIC, NEN, SCA, NWS, NES, SAM, ESAF, ESB, WCA, ECA, TIB, EAS, ARP, SEA, NAU, CAU	16	36.4%
Wet anomalies intensify, dry anomalies weaken	WNA, CNA, ENA, CAR, SES, NEU, WCE, EEU, MED, SEAF, RAR, WSB, RFE, NZ	14	31.8%
Wet anomalies weaken, dry anomalies intensify	SWS, WAF, WSAF	3	6.8%
Both wet and dry anomalies weaken	NWN, SAU	2	4.5%
At least one side is not significant	NCA, NSA, SSA, SAH, CAF, NEAF, MDG, SAS, EAU	9	20.5%

The full names and attributes corresponding to the IPCC AR6 regional abbreviations are provided in Table S1 of the Supplementary Material

precipitation anomalies have generally exhibited a concurrent intensification of wet and dry extremes. This indicates that the statistical distribution of annual precipitation anomalies has expanded toward stronger positive and negative anomalies. Such changes are reflected not only in increasing return levels, but also in the more frequent occurrence of events with the same return period in recent decades, suggesting that global extreme hydroclimatic risk has increased in both intensity and occurrence frequency.

Beyond the globally averaged signal, the spatial and regional analyses reveal pronounced regional heterogeneity in the changes in precipitation anomalies. The responses differ substantially among regions and return periods. The intensification of wet anomalies is mainly concentrated in the mid- to high-latitudes and monsoon-affected regions, whereas the intensification of dry anomalies occurs more frequently in parts of the low latitudes and subtropical regions. Both the 10-year and 50-year events show a consistent spatial pattern of enhanced wet anomalies and intensified dry anomalies. However, the 10-year events are characterized by broader spatial coverage, whereas the 50-year events affect a relatively smaller area but exhibit stronger local changes. Together with previous findings on the influence of the AMOC on Northern Hemisphere land precipitation, the cross-hemispheric modulation of Northern Hemisphere winter precipitation by the Southern Annular Mode, and the combined effects of tropical-South Pacific SST anomalies and the NAO on regional precipitation, the above regional differences suggest that the spatial responses of extreme precipitation anomalies may be related to large-scale ocean circulation, atmospheric teleconnections, and air-sea coupled variability (Nan and Li 2003; Liu et al. 2015; Zhang et al. 2021; Tang and Li 2024).

Overall, global extreme precipitation anomalies over the past century are characterized by increasing event intensity, more frequent occurrence of events with the same return period, and substantial spatial heterogeneity. Future research will proceed in three steps. First, regions exhibiting a pronounced two-sided expansion of wet and dry precipitation anomalies will be selected, and T-year wet and dry events will be identified using a full-record fixed-threshold approach, ensuring that all event years are selected according to a common intensity criterion. This framework can also be applied separately to different seasons to identify season-specific extreme precipitation events. Second, composite and moisture-budget analyses will be conducted to compare the common physical characteristics of wet and dry events, focusing on local moisture conditions, land–atmosphere interactions, moisture transport, and circulation anomalies. Third, the same return-period framework will be extended to potential drivers, including regional circulation indices and sea-surface temperature anomalies, to examine their temporal correspondence and lead-lag relationships with precipitation-event years. Comparisons across different periods or moving windows will further determine whether these relationships vary with the background climate and

Table 3 Baseline return levels (mm), mean critical intensities (mm), and relative changes (%) of 10-year extreme wet and dry annual precipitation anomaly events across IPCC AR6 reference regions relative to the reference period (1891–1940)

Subregions		Wet events			Dry events		
No	Region	Baseline RL	Mean CI	Relative Change (%)	Baseline RL	Mean CI	Change (%)
1	GIC	29.03	51.92	78.84	− 32.66	− 35.59	8.98
2	NWN	26.8	36.85	37.54	− 20.6	− 36.44	76.89
3	NEN	13.86	26.95	94.37	− 17.17	− 25.82	50.43
4	WNA	73.4	82.62	12.56	− 79.47	− 72.83	− 8.36
5	CNA	109.56	142.19	29.78	− 109.89	− 103.15	− 6.13
6	ENA	73.27	111.19	51.76	− 76.91	− 51.9	− 32.52
7	NCA	71.93	88.6	23.18	− 58.38	− 68.69	17.66
8	SCA	137.03	165.72	20.93	− 118.3	− 197.37	66.84
9	CAR	184.88	190.81	3.21	− 115.91	− 148.57	28.18
10	NWS	66.44	152.41	129.41	− 37.63	− 129.94	245.35
11	NSA	74.3	149.22	100.83	− 77.48	− 147.68	90.6
12	NES	168.65	208.23	23.47	− 124.11	− 215.13	73.33
13	SAM	14.6	85.74	487.19	− 10.55	− 107.92	923.2
14	SWS	76.95	69.91	-9.14	− 77.08	− 113.14	46.79
15	SES	69.7	134.91	93.56	− 87.52	− 84.26	− 3.72
16	SSA	60.75	61.51	1.26	− 62.06	− 76.93	23.96
17	NEU	57.49	91.28	58.78	− 52.98	− 52.6	− 0.71
18	WCE	83.88	90.41	7.78	− 84.61	− 78.15	− 7.63
19	EEU	54.5	73.39	34.67	− 63.43	− 44.22	− 30.29
20	MED	46.47	54.15	16.54	− 34.59	− 53.16	53.7
21	SAH	14.08	19.84	40.87	− 8.31	− 18.75	125.77
22	WAF	97.36	100.42	3.14	− 95.33	− 163.15	71.14
23	CAF	61.81	89.14	44.21	− 36	− 74.03	105.65
24	NEAF	66.76	59	-11.61	− 63.74	− 57.21	− 10.24
25	SEAF	105.24	143.76	36.6	− 95.79	− 108.5	13.26
26	WSAF	55.01	82.63	50.2	− 42.45	− 78.53	85.01
27	ESAF	102.94	111.2	8.02	− 99.25	− 120.87	21.79
28	MDG	129.15	185.83	43.88	− 93.7	− 180.75	92.89
29	RAR	10.63	29.62	178.54	− 18.53	− 26.87	44.96
30	WSB	28.14	43.63	55.07	− 30.34	− 32.22	6.18
31	ESB	12.65	27.28	115.66	− 13.36	− 20.62	54.35
32	RFE	30.13	68.3	126.65	− 37.15	− 51.54	38.72
33	WCA	21.14	42.37	100.45	− 26.5	− 30.91	16.64
34	ECA	10.36	21.54	108.04	− 8.96	− 14.17	58.09
35	TIB	39.61	39.86	0.62	− 36.46	− 42.07	15.39
36	EAS	74.18	94.79	27.78	− 69.96	− 76.68	9.6
37	ARP	3.95	20.41	416.22	− 3.5	− 14.33	309.24
38	SAS	125.07	116.1	-7.17	− 101.15	− 103.01	1.84
39	SEA	170.71	197.36	15.61	− 206.94	− 246.97	19.34
40	NAU	172.42	236.24	37.01	− 185.05	− 190.78	3.1
41	CAU	60.85	106.87	75.63	− 52.44	− 66.05	25.97
42	EAU	154.21	202.29	31.17	− 224.49	− 214.29	− 4.54
43	SAU	71.23	100.27	40.77	− 56.9	− 86.6	52.18
44	NZ	106.39	119.6	12.42	− 155.77	− 146.76	− 5.79

RL = return level; CI = critical intensity. Relative change is calculated as (|Mean CI|−|Baseline RL|)/|Baseline RL|×100%. Positive and negative values indicate an increase and a decrease, respectively, in the absolute magnitude of the mean critical intensity relative to the baseline return level

Table 4 Same as Table 3, but for 50-year events

Subregions		Wet events			Dry events		
No	Region	Baseline RL	Mean CI	Relative Change (%)	Baseline RL	Mean CI	Change (%)
1	GIC	43.25	92.17	113.08	− 54.14	− 72.74	34.37
2	NWN	85.24	78.69	− -7.68	− 34.25	− 69.81	103.81
3	NEN	24.55	42.44	72.88	− 34.04	− 45.74	34.39
4	WNA	114.77	160.7	40.02	− 129.46	− 122.94	− 5.03
5	CNA	191.5	221.36	15.59	− 184.19	− 160.95	− 12.62
6	ENA	114.23	165.24	44.65	− 142.7	− 114.54	− 19.73
7	NCA	120.85	197.37	63.31	− 115.89	− 117.44	1.34
8	SCA	272.48	292.63	7.39	− 177.97	− 271.55	52.58
9	CAR	264.35	281.57	6.51	− 220.26	− 220.37	0.05
10	NWS	106	281.11	165.21	− 181.32	− 233.39	28.72
11	NSA	152	280.68	84.66	− 197.58	− 255.47	29.3
12	NES	402.88	464.25	15.23	− 314.36	− 343.29	9.2
13	SAM	42.86	152.75	256.41	− 50.94	− 217.6	327.16
14	SWS	207.33	163.17	− 21.3	− 134.8	− 167.15	23.99
15	SES	161.17	219.88	36.42	− 140.11	− 158.96	13.45
16	SSA	115.36	175.71	52.31	− 79.76	− 104.8	31.39
17	NEU	95.7	130.15	36.01	− 114.03	− -102.19	− 10.39
18	WCE	104.92	126.25	20.33	− 160.2	− 126.35	− 21.13
19	EEU	120.68	121.84	0.96	− 76.69	− 71.34	− 6.98
20	MED	54.63	82.01	50.12	− 50.38	− 91.35	81.35
21	SAH	23.26	39.05	67.86	− 14.31	− 28.62	100.07
22	WAF	160.65	144.1	− 10.3	− 168.94	− 268.57	58.97
23	CAF	127.99	144.93	13.24	− 96.69	− 148.16	53.23
24	NEAF	117.31	120.4	2.63	− 112.75	− 123.04	9.13
25	SEAF	131.81	313.63	137.94	− 223.39	− 201.75	− 9.69
26	WSAF	168.62	161.64	− 4.14	− 100.46	− 119.87	19.32
27	ESAF	189.44	207.83	9.71	− 160.31	− 188.51	17.59
28	MDG	264.67	320.18	20.97	− 346.3	− 289.94	− 16.28
29	RAR	12.7	74.73	488.24	− 48.49	− 53.27	9.86
30	WSB	50.32	70.16	39.43	− 57.48	− 60.37	5.03
31	ESB	37.08	53.43	44.09	− 28.16	− 36.15	28.37
32	RFE	44.62	103.7	132.4	− 80.11	− 94.47	17.93
33	WCA	33.7	61.01	81.03	− 43.72	− 48.75	11.5
34	ECA	25.89	40.58	56.72	− 17.8	− 30.37	70.67
35	TIB	56.6	58.05	2.57	− 52.84	− 56.64	7.19
36	EAS	132.41	188.24	42.17	− 107.26	− 115.46	7.64
37	ARP	9.11	44.14	384.5	− 4.23	− 24.2	471.64
38	SAS	167.97	185.94	10.7	− 123.22	− 168.51	36.76
39	SEA	271.34	295.6	8.94	− 396.07	− 452.37	14.22
40	NAU	322.51	413.83	28.32	− 265.04	− 289.85	9.36
41	CAU	100.93	227.67	125.56	− 84.72	− 90.44	6.75
42	EAU	369.54	520.02	40.72	− 400.8	− 332.72	− 16.99
43	SAU	195.9	190.17	− 2.93	− 164.37	− 156.07	− 5.05
44	NZ	158.39	202.62	27.93	− 236.48	− 208.78	− 11.71

RL, CI, and relative change are defined as in Table 3

help identify potential precursor signals, thereby deepening our understanding of the physical causes of changes in extreme precipitation anomalies and their implications for regional risk.

Supplementary Information The online version contains supplementary material available at https://doi.org/10.1007/s00382-026-08378-8.

Acknowledgments The authors are grateful to Xiaowen Zhu for her assistance with code modification and checking, and to Yulian Fu and Yanbing Zhu for their helpful discussions and suggestions. This research was supported by the National Natural Science Foundation of China (42288101), Laoshan Laboratory (No.LSKJ202202600), and Fundamental Research Funds for the Central Universities (202242001, 202515028).

Author contributions JL conceived the study, proposed the theoretical framework, supervised the research, and finalized the manuscript. YT performed the main analysis, produced the figures, interpreted the results, and drafted the manuscript. WB refined the theoretical framework. All authors discussed, reviewed, and revised the manuscript.

Funding This work is jointly supported by the National Natural Science Foundation of China (42288101), Laoshan Laboratory (No. LSKJ202202600), and Fundamental Research Funds for the Central Universities (202242001, 202515028).

Data availability The GPCC Full Data Monthly Product Version 2022 at 2.5° was obtained from the GPCC/DWD data portal (https://opendata.dwd.de/climate_environment/GPCC/html/fulldata-monthly_v2022_doi_download.html). The CRU TS v4.05 monthly precipitation dataset was obtained from the Climatic Research Unit data portal (https://crudata.uea.ac.uk/cru/data/hrg/cru_ts_4.05/) and was used to assess the consistency of the main conclusions across datasets.

Declarations

Conflict of interest The authors have no relevant financial or non-financial interests to disclose.

References

Alexander LV, Zhang X, Peterson TC et al (2006) Global observed changes in daily climate extremes of temperature and precipitation. J Geophys Res Atmos 111:D05109. https://doi.org/10.1029/2005JD006290

Ban W, Li JP (2026) The unified extreme value theory for characterizing changes in return periods and levels of N-year temperature anomalies. Clim Dyn 64:352. https://doi.org/10.1007/s00382-026-08315-9

Becker A, Finger P, Meyer-Christoffer A, Rudolf B, Schamm K, Schneider U, Ziese M (2013) A description of the global land-surface precipitation data products of the global precipitation climatology centre with sample applications including centennial (trend) analysis from 1901–present. Earth Syst Sci Data 5:71–99. https://doi.org/10.5194/essd-5-71-2013

Benestad RE, Lussana C, Dobler A (2024) Global record-breaking recurrence rates indicate more widespread and intense surface air temperature and precipitation extremes. Sci Adv 10(45):eado3712. https://doi.org/10.1126/sciadv.ado3712

Chen LZ, Brun P, Buri P et al (2025) Global increase in the occurrence and impact of multiyear droughts. Sci 387:278–284. https://doi.org/10.1126/science.ado4245

Devò P, Caruso MF, Borga M, Marani M (2025) Estimates of rare rainfall extremes in ungauged areas. Geophys Res Lett 52:e2024GL113576. https://doi.org/10.1029/2024GL113576

Donat MG, Alexander LV, Yang H et al (2013) Updated analyses of temperature and precipitation extreme indices since the beginning of the twentieth century: the HadEX2 dataset. J Geophys Res Atmos 118:2098–2118. https://doi.org/10.1002/jgrd.50150

Donat MG, Lowry AL, Alexander LV et al (2016) More extreme precipitation in the world's dry and wet regions. Nat Clim Chang 6:508–513. https://doi.org/10.1038/nclimate2941

Dunn RJH, Herold N, Alexander LV et al (2024) Observed global changes in sector-relevant climate extremes indices-an extension to HadEX3. Earth Space Sci 11:e2023EA003279. https://doi.org/10.1029/2023EA003279

Fan XW, Zhang YL, Shi K, Peng J et al (2024) Surging compound drought-heatwaves underrated in a warming climate. Proc Natl Acad Sci U S A 121:e2410294121. https://doi.org/10.1073/pnas.2410294121

Gebrechorkos SH, Sheffield J, Vicente-Serrano SM et al (2025) Warming accelerates global drought severity. Nature 642:628–635. https://doi.org/10.1038/s41586-025-09047-2

Gründemann GJ, Zorzetto E, Beck HE et al (2023) Extreme precipitation return levels for multiple durations on a global scale. J Hydrol 621:129558. https://doi.org/10.1016/j.jhydrol.2023.129558

Harris I, Osborn TJ, Jones P, Lister D (2020) Version 4 of the CRU TS monthly high-resolution gridded multivariate climate dataset. Sci Data 7:109. https://doi.org/10.1038/s41597-020-0453-3

He N, Yin JB, Liu P, Fu X, Zhang Q, Cheng L, Moulds S, Volchak A (2025) Global increases in dry-wet abrupt alternation events under climate change. Geophys Res Lett 52:e2025GL117322. https://doi.org/10.1029/2025GL117322

Held IM, Soden BJ (2006) Robust responses of the hydrological cycle to global warming. J Clim 19:5686–5699. https://doi.org/10.1175/JCLI3990.1

Huang JP, Yu HP, Dai AG, Wei Y, Kang LT (2017) Drylands face potential threat under 2 °C global warming target. Nat Clim Chang 7:417–422. https://doi.org/10.1038/nclimate3275

IPCC (2021) Climate change 2021: the physical science basis. Contribution of working group I to the sixth assessment report of the Intergovernmental Panel on Climate Change. Cambridge University Press, Cambridge. https://doi.org/10.1017/9781009157896

Iturbide M, Gutiérrez JM, Alves LM et al (2020) An update of IPCC climate reference regions for subcontinental analysis of climate model data: definition and aggregated datasets. Earth Syst Sci Data 12:2959–2970. https://doi.org/10.5194/essd-12-2959-2020

Jorgensen SK, Nielsen-Gammon JW (2024) Nonstationarity in extreme precipitation return values along the U.S. Gulf Southeastern Coast. J Hydrometeorol 5:771–788. https://doi.org/10.1175/JHM-D-22-0157.1

Katz RW, Parlange MB, Naveau P (2002) Statistics of extremes in hydrology. Adv Water Resour 25:1287–1304. https://doi.org/10.1016/S0309-1708(02)00056-8

Kharin VV, Zwiers FW (2005) Estimating extremes in transient climate change simulations. J Clim 18:1156–1173. https://doi.org/10.1175/JCLI3320.1

Li C, Liu JY, Du FJ, Zwiers FW, Feng GL (2025) Increasing certainty in projected local extreme precipitation change. Nat Commun 16:850. https://doi.org/10.1038/s41467-025-56235-9

Li J, Zhao Y, Li JP, Guo LY, Shen C, Zhang LJ, Deng L, Chen DD (2026) Deciphering the shift in extreme precipitation over the lower reaches of the Yangtze River Basin: a synoptic-scale analysis. Clim Dyn 64:98. https://doi.org/10.1007/s00382-026-08059-6

Liu T, Li JP, Zheng F (2015) Influence of the boreal autumn Southern Annular Mode on winter precipitation over land in the Northern Hemisphere. J Clim 28:8825–8839. https://doi.org/10.1175/JCLI-D-14-00704.1

Nan SL, Li JP (2003) The relationship between the summer precipitation in the Yangtze River valley and the boreal spring Southern Hemisphere annular mode. Geophys Res Lett 30:2266. https://doi.org/10.1029/2003GL018381

O'Gorman PA (2015) Precipitation extremes under climate change. Curr Clim Change Rep 1:49–59. https://doi.org/10.1007/s40641-015-0009-3

Schneider U, Hänsel S, Finger P, Rustemeier E, Ziese M. (2022) GPCC full data monthly product version 2022 at 2.5°: monthly land-surface precipitation from rain-gauges built on GTS-based and historical data. Deutscher Wetter-dienst. https://doi.org/10.5676/DWD_GPCC/FD_M_V2022_250

Su J, Ding YH, Liu YJ, Wang J, Zhang YX (2024) China is suffering from fewer but more severe drought to flood abrupt alternation events. Weather Clim Extrem 46:100737. https://doi.org/10.1016/j.wace.2024.100737

Sun QH, Zhang XB, Zwiers FW et al (2021) A global, continental, and regional analysis of changes in extreme precipitation. J Clim 34:243–258. https://doi.org/10.1175/JCLI-D-19-0892.1

Sun Y, Li JP, Wang H, Li RZ, Tang XX (2023) Extreme rainfall in Northern China in September 2021 tied to air–sea multi-factors. Clim Dyn 60:1987–2001. https://doi.org/10.1007/s00382-022-06439-2

Tan XZ, Wu XX, Huang ZQ, Fu JY et al (2023) Increasing global precipitation whiplash due to anthropogenic greenhouse gas emissions. Nat Commun 14:2796. https://doi.org/10.1038/s41467-023-38510-9

Tang X, Li JP. 2024 Synergistic effect of boreal autumn SST over the tropical and South Pacific and winter NAO on winter precipitation in the southern Europe. npj Climate Atmos Sci 7(1):78. https://doi.org/10.1038/s41612-024-00628-y

Trenberth KE (2011) Changes in precipitation with climate change. Clim Res 47:123–138. https://doi.org/10.3354/cr00953

Trenberth KE, Asrar GR (2014) Challenges and opportunities in water cycle research: WCRP contributions. Surv Geophys 35:515–532. https://doi.org/10.1007/s10712-012-9214-y

Vicente-Serrano SM, Beguería S, López-Moreno JI (2010) A multiscalar drought index sensitive to global warming: the standardized precipitation evapotranspiration index. J Clim 23:1696–1718. https://doi.org/10.1175/2009JCLI2909.1

Wehner MF, Duffy ML, Risser M, Paciorek CJ, Stone DA, Pall P (2024) On the uncertainty of long-period return values of extreme daily precipitation. Front Clim 6:1343072. https://doi.org/10.3389/fclim.2024.1343072

Westra S, Alexander LV, Zwiers FW (2013) Global increasing trends in annual maximum daily precipitation. J Clim 26:3904–3918. https://doi.org/10.1175/JCLI-D-12-00502.1

Wu ZW, Li JP, He JH, Jiang ZH (2006a) Large-scale atmospheric singularities and summer long-cycle droughts-floods abrupt alternation in the middle and lower reaches of the Yangtze River. Chin Sci Bull 51:2027–2034. https://doi.org/10.1007/s11434-006-2060-x

Wu ZW, Li JP, He JH, Jiang ZH (2006b) Occurrence of droughts and floods during the normal summer monsoons in the mid- and lower reaches of the Yangtze River. Geophys Res Lett 33:2005GL024487. https://doi.org/10.1029/2005GL024487

Xie QY, Li JP, Zhao YF (2020) Effects of air temperature and precipitation on soil moisture on the Qinghai-Tibet Plateau during the 2015 growing season. Adv Meteorol 2020:4918945. https://doi.org/10.1155/2020/4918945

Yate TA, Ren GY (2025) An overview of observed changes in precipitation totals and extremes over global land, with a focus on Africa. Earth-Sci Rev 262:105063. https://doi.org/10.1016/j.earscirev.2025.105063

Zhang J, Liu YS, Sun C, Li JP, Ding RQ, Xie F, Xie TJ, Zhang YZ, Gong ZQ (2021) On the connection between AMOC and observed land precipitation in Northern Hemisphere: a comparison of the AMOC indicators. Clim Dyn 56:651–664. https://doi.org/10.1007/s00382-020-05496-9

Zhang LM, Yuan F, He XG (2024a) Probabilistic assessment of global drought recovery and its response to precipitation changes. Geophys Res Lett 51:e2023GL106067. https://doi.org/10.1029/2023GL106067

Zhang WX, Zhou T, Wu PL (2024b) Anthropogenic amplification of precipitation variability over the past century. Science 385:427–432. https://doi.org/10.1126/science.adp0212

Zhao Y, Li JP, Tian Y, Li J (2024) Distinguishing extreme precipitation mechanisms associated with atmospheric rivers and nonatmospheric rivers in the lower Yangtze River Basin. J Clim 37:3659–3678. https://doi.org/10.1175/JCLI-D-23-0400.1

Zhuang YZ, Fu R, Lisonbee J et al (2024) Anthropogenic warming has ushered in an era of temperature-dominated droughts in the western United States. Sci Adv 10(45):eadn9389. https://doi.org/10.1126/sciadv.adn9389